Journal of Biomechanics 82 (2019) 142–148

Contents lists available at ScienceDirect

Journal of Biomechanics

journal homepage: www.elsevier.com/locate/jbiomech
www.JBiomech.com

Influence of altered geometry and material properties on tissue stress distribution under load in tendinopathic Achilles tendons – A subject-specific finite element analysis

Vickie B. Shim [b,*], Wencke Hansen [a], Richard Newsham-West [a], Leila Nuri [a], Steven Obst [c], Claudio Pizzolato [a], David G. Lloyd [a], Rod S. Barrett [a]

[a] Menzies Health Institute Queensland, Griffith University, Gold Coast Campus, Australia
[b] Auckland Bioengineering Institute, University of Auckland, Auckland, New Zealand
[c] School of Health, Medical and Applied Sciences, Central Queensland University, Australia

ARTICLE INFO

Article history:
Accepted 20 October 2018

Keywords:
Ultrasound
Tendinopathy
Young's modulus
Cross-sectional area
Strain
von Mises

ABSTRACT

Achilles tendon material properties and geometry are altered in Achilles tendinopathy. The purpose of this study was to determine the relative contributions of altered material properties and geometry to free Achilles tendon stress distribution during a sub-maximal contraction in tendinopathic relative to healthy tendons. Tendinopathic (n = 8) and healthy tendons (n = 8) were imaged at rest and during a sub-maximal voluntary isometric contraction using three-dimensional freehand ultrasound. Images were manually segmented and used to create subject-specific finite element models. The resting cross-sectional area of the free tendon was on average 31% greater for the tendinopathic compared to healthy tendons. Material properties for each tendon were determined using a numerical parameter optimisation approach that minimised the difference in experimentally measured longitudinal strain and the strain predicted by the finite element model under submaximal loading conditions for each tendon. The mean Young's modulus for tendinopathic tendons was 53% lower than the corresponding control value. Finite element analyses revealed that tendinopathic tendons experience 24% less stress under the same sub-maximal external loading conditions compared to healthy tendons. The lower tendon stress in tendinopathy was due to a greater influence of tendon cross-sectional area, which alone reduced tendon stress by 30%, compared to a lower Young's modulus, which alone increased tendon stress by 8%. These findings suggest that the greater tendon cross-sectional area observed in tendinopathy compensates for the substantially lower Young's modulus, thereby protecting pathological tendon against excessive stress.

1. Introduction

Achilles tendinopathy is a common tendon injury which is prevalent in, but not exclusive to, athletic populations (Kongsgaard et al., 2005; Rolf and Movin, 1997). Up to 25% of affected patients will eventually require operative treatment and 20% of those undergo further surgery (Alfredson, 2003). Achilles tendinopathy is most commonly located in the mid-portion of the free tendon, 2–6 cm from the calcaneal insertion (Astrom and Rausing, 1995; Maffulli et al., 2004; Rolf and Movin, 1997) and is characterised by collagen bundle disruption, hyper-cellularity, hyper-vascularity and altered collagen, glycosaminoglycan and fluid content (Khan et al., 1999). Tendinopathy has also been reported to cause a reduction in tendon mechanical and material properties (Arya and Kulig, 2010; Helland et al., 2013). For the Achilles tendon, stiffness was reduced by 20% and Young's modulus by 50% relative to healthy tendons (Arya and Kulig, 2010). For a tendon of a given length, a lower stiffness would result in greater tendon strain under the same external load. A further adaptation in Achilles tendinopathy is tendon thickening, which increases the tendon cross-sectional area (CSA) by 20–66% (Arya and Kulig, 2010; Helland et al., 2013; Leung and Griffith, 2008; Nuri et al., 2017b, 2018; Obst et al., 2018). Tendon thickening may therefore be an adaptation that at least partially compensates for the reduction in tendon stiffness, thereby protecting the tendon from high strains. For a given external load, an increased tendon CSA would also be expected to decrease the net tendon stress. In the study by Arya and Kulig (2010), peak Achilles tendon stress (force/CSA) was approximately half in tendinopathic compared to healthy Achilles tendons, primarily due to much larger CSA in tendinopathy. However, it is currently unclear how altered subject-specific

* Corresponding author.
E-mail address: v.shim@auckland.ac.nz (V.B. Shim).

https://doi.org/10.1016/j.jbiomech.2018.10.027
0021-9290/

material properties, localised geometry, and their interaction affect the stress distribution of tendinopathic Achilles tendons.

Localised stress of healthy Achilles tendons have been assessed using subject-specific finite element (FE) models as the relative effects of variations in tendon geometry and material properties on localised tendon stress cannot be assessed experimentally. Shim and colleagues (Shim et al., 2014) combined three-dimensional reconstructions of the Achilles tendon geometry from transverse ultrasound images with corresponding load-elongation data of fresh-frozen cadaver tendons and reported that tendon stress distributions during loading were more sensitive to variations in tendon geometry than variations in material properties. Similarly, Hansen et al. (2017) reported that in-vivo free Achilles tendon stress magnitude was more influenced by tendon geometry than material properties. Shim et al. (Shim et al., 2018) further reported that the Achilles tendon may experience non-uniform tissue deformation between tendon regions when in vivo measures of sub-tendon geometry and tendon twist were incorporated in their FE model. Taken together, the abovementioned FE studies suggest that the mechanical behaviour of the healthy Achilles tendon under load is particularly sensitive to tendon geometry. However, these results cannot be generalised to tendinopathic Achilles tendons, which are characterised by alteration in both geometry and material properties.

The purpose of this study was to determine the relative contribution of altered geometry and material properties to tendon stress in tendinopathic compared to healthy free Achilles tendons. We hypothesised that the larger CSA in tendinopathic Achilles tendons would have a greater influence on tissue stress distribution than the reduction in stiffness, thereby resulting in an overall stress reduction.

2. Methods

2.1. Participant characteristics

Eight participants with mid-portion Achilles tendinopathy (6 males, 2 females; age: 37 ± 11 years, height: 177 ± 9 cm, weight: 78 ± 13 kg) and 8 age-matched controls with normal, healthy Achilles tendons (5 males, 3 females; age: 29 ± 4 years, height: 180 ± 6 cm, weight: 75 ± 14 kg) participated in the study. The eligibility criteria for the tendinopathy group were symptomatic mid-potion Achilles tendinopathy (self-reported tendon pain, tenderness to palpation, focal thickening), minimum duration of symptoms of 3 months, and a Victorian Institute of Sports Assessment–Achilles tendon (VISA-A) score of less than 80 points (Robinson et al., 2001). Potential participants were excluded if they had insertional tendinopathy, neurological or musculoskeletal conditions affecting the lower limbs, or had undergone lower limb surgery. The study was approved by the Institutional Human Research Ethics Committee and all relevant ethical guidelines, including provision of a written informed consent prior to participation in the study, were followed.

2.2. Experimental data collection and analysis procedures

All data were collected from the right Achilles tendon of each participant, who were positioned prone with knee extended and ankle in neutral position rigidly fixed to an isometric dynamometer (TFF600, Futek, Irvine, CA, USA). Particular care was taken in order to align ankle and dynamometer axes of rotation. Tendon was preconditioned following a standardised procedure, which included two sub-maximal contractions followed by four maximal contractions (Nuri et al., 2017a). Maximum voluntary isometric contraction (MVIC) torque was then determined as the greatest ankle plantarflexion torque generated from 3 MIVC trials, which involved ramped isometric contraction over 3–5 s with 1–2 min of rest. Three-dimensional freehand ultrasound (Barber et al., 2009) was used for tendon imaging at rest and during submaximal contractions held for approximately 30 s. The contraction intensity was 70%MVIC for participants with healthy tendons. A contraction intensity of 50% MVIC was chosen for participants with tendinopathic tendons to ensure they could complete the task without excessive discomfort. Real-time visual feedback of torque was provided to ensure the ankle torque was kept within ±5% of the target load.

The three-dimensional ultrasound system consisted of a two-dimensional ultrasound (SonixTouch, Ultrasonix, Richmond, British Columbia, Canada) combined with a five-camera optical tracking system (Optitrack V100:R2, Tracking Tools v2.5.2, NaturalPoint, Corvallis, OR, USA) with tracking accuracy <1 mm. All scans were performed by a single investigator using a single transverse sweep between the osteotendinous insertion and the musculotendinous junction. Ultrasound images were acquired using a 58-mm linear transducer with a central frequency of 10 MHz, sampling frequency of 40 Hz and standardised B-mode image settings. The two-dimensional images were spatially aligned using Stradwin software (Version 5.2) to form a reconstructed image stack. The three-dimensional point accuracy of spatial calibrations using an optical tracking system has been reported to be less than 1 mm (Hsu et al., 2006; Treece et al., 2003). Prior studies have established the validity and repeatability of the three-dimensional ultrasound system for in vivo measurement of Achilles free tendon morphology (length, volume, CSA, AP diameter and ML diameter) under passive and active loading conditions (Obst et al., 2014a; Obst et al., 2014b). Free Achilles tendon volume reconstructions were performed based on at least 6 segmented cross-sections using the volume algorithms provided in Stradwin (Treece et al., 1999) (Fig. 1). The average CSA of the free tendon was obtained from the ratio of measured free tendon volume to free tendon length.

2.3. Mesh generation

The surface geometries of each free AT were imported from Stradwin into 3matics 9.0 (Materialise, Leuven, Belgium). The longitudinal axes of inertia were aligned with the x-axis of the global coordinate system and point cloud data subsequently exported to the FE analysis software Continuum Mechanics Image analysis, Signal processing and System Identification (CMISS) (www.cmiss.org, freely available for academic use).

A point cloud describing the free AT surface geometry for a separate healthy participant (female, 32 years, 177 cm, 64 kg) was generated from a transverse, high-accuracy magnetic resonance imaging scan (Philips Ingenia 3T, slice thickness 3.5 mm, voxel size 0.6 mm × 0.6 mm, 50 slices, slice gap 0.3 mm) using the software Mimics (Research 17.0, Materialise, Leuven, Belgium). The point cloud was used to create a generic finite element mesh made up of three-dimensional cubic Hermite element in CMISS, which was then morphed to match the subject-specific mesh of each participants Achilles tendon using the freeform deformation method (Shim et al., 2016). The average root mean square (RMS) error between the subject-specific point cloud and the morphed mesh was 0.21 ± 0.07 mm. Element distortions occurred during morphing were removed via manual adjustment. An average free tendon geometry was computed for all healthy (n = 8) and tendinopathic tendons (n = 8) and used for subsequent analysis.

2.4. Boundary conditions, material properties and finite element analysis

Force boundary conditions were derived from the measured ankle plantarflexion torque divided by a generic ankle joint moment arm (Kongsgaard et al., 2011). The direction of the force

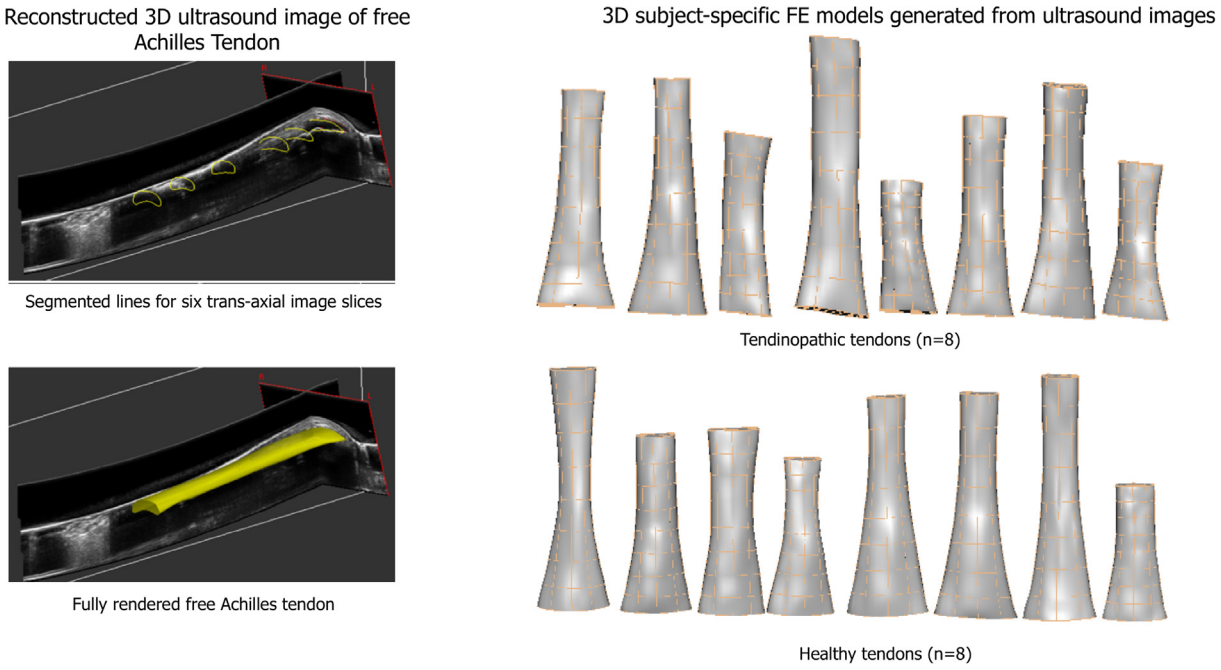

Fig. 1. (Left) Reconstructed three-dimensional ultrasound image of the free Achilles tendon showing (Top) segmentation lines for six *trans*-axial image slices, and (Bottom) fully rendered free Achilles tendon. (Right) Final finite element meshes of tendinopathic (Top) and healthy (Bottom) tendons.

vector was derived from individual muscle volumes of the Triceps Surae based on one subject's magnetic resonance imaging scan (Fig. 2). The resulting boundary load was equally distributed across the 11 nodes of the proximal face. The nodes in the distal face were fixed.

The free Achilles tendon was treated as incompressible, transversely isotropic and hyperelastic tissue (Hansen et al., 2017; Shim et al., 2014) based on the exponential strain energy function for hyperelastic material developed by Weiss et al. (1996). This formulation has five coefficients (c_1–c_5). Values c_2 and c_3 were fixed. As the ground substance matrix was considered a Neo-Hookean material, c_2 was set to 0. The scaling parameter of the strain energy functionc_3 was obtained from literature(Shim et al., 2014) and set to 19.4. The remaining three parameters were optimised. c_1 describes the scaling of ground substance, c_4 describes the rate of the collagen fibre loading and c_5 represents the Young's modulus. While c_4 describes the tendon behaviour in the toe region, c_5 influences the behaviour in the tendon's elastic, linear region. The mate-

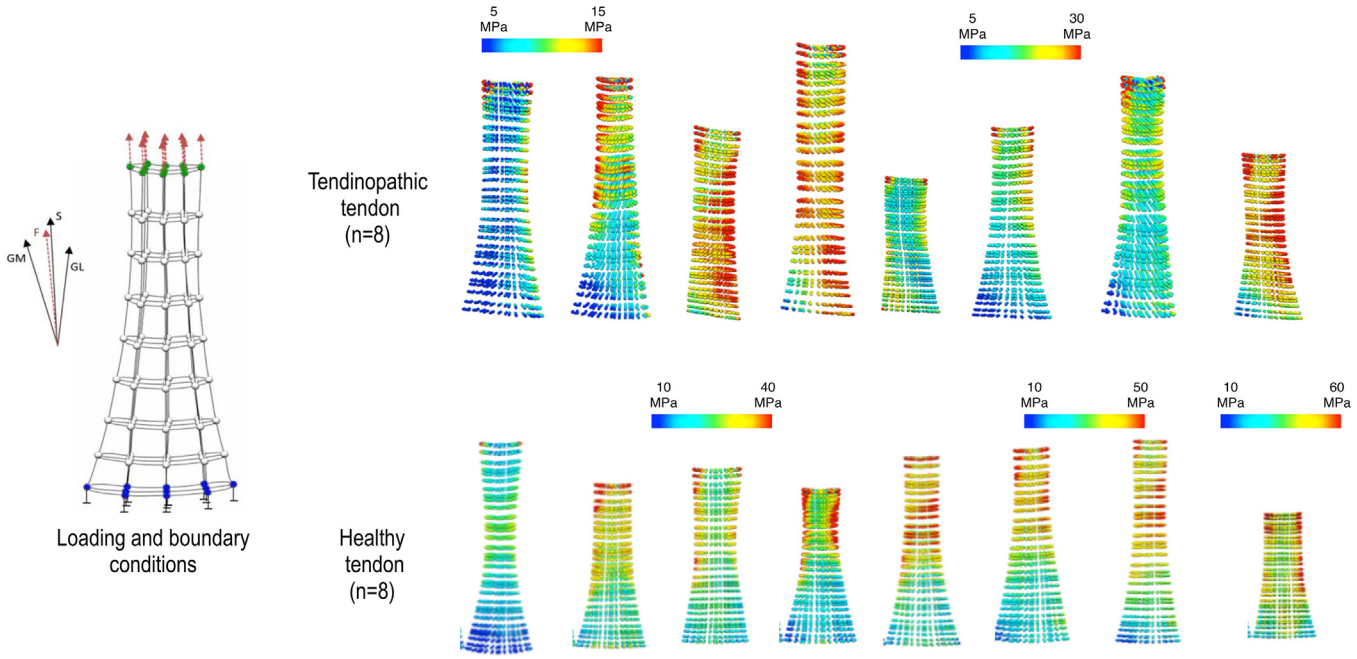

Fig. 2. (Left) A diagram showing the applied boundary and loading conditions. Applied force vectors were computed from individual force vectors of Soleus (S), Gastrocnemius Medialis (GM) and Gastrocnemius Lateralis (GL). The force was assigned to the nodes of the proximal face (green) and the displacement boundary condition was assigned to the nodes of the distal face (blue). (Right) Von Mises stress [MPa] for tendinopathic tendons under subject-specific 50% MVIC load with subject-specific geometry and material properties (Top row) and healthy tendons under subject-specific 70% MVIC load with subject-specific geometry and material properties. Red (blue) indicates the greatest (lowest) stress. (For interpretation of the references to colour in this figure legend, the reader is referred to the web version of this article.)

rial parameter optimization was performed using the non-linear least squares *lsqnonlin* algorithm in Matlab's optimisation tool box (The MathWorks, USA), as per our previous studies (Hansen et al., 2017; Shim et al., 2014). The optimization routine iteratively altered the values of parameters c_1, c_4, and c_5 for the unloaded AT mesh to minimise the difference between FE predicted shape of the AT and the experimental AT shape obtained from ultrasound images during the 50%MVIC contraction. Multiple initial parameter guesses were used to ensure a global minima was found for each tendon. Details of the parameter optimization process can be found in our previous works (Hansen et al., 2017; Shim et al., 2014).

2.5. Stress analysis

Internal tissue stress was initially computed at more than 4000 internal data points located at numerical integration points called Gauss points for each subject-specific tendon geometry and corresponding subject-specific material properties at a load corresponding to the 70%MVIC condition for the healthy ATs (Fig. 2) measured from the experiments. The average values for measured torques for healthy and tendinopathic AT are given in Table 1. High stresses in the regions where boundary conditions were applied were not included in accordance with Saint-Venant's principle (Horgan and Knowles, 1983).

von Mises stresses were subsequently computed for different combinations of average healthy and average tendinopathic geometry and material properties at a load corresponding to the 70% MVIC condition for the healthy ATs. The influence of tendinopathic material properties on the internal stress distribution of the free tendon was examined by plotting stress distributions based on average tendinopathic material properties against stress distributions from average healthy material properties both using average healthy geometry. The influence of tendinopathic geometry on internal stress distribution was examined by plotting stress distributions from average tendinopathic geometry against average healthy geometry both using average healthy material properties. The combined effect of average tendinopathic geometry and material properties on localised free AT stress was also investigated by plotting against stress distributions from average healthy geometry and material properties. A further analysis was performed to examine how subject-specific compared to average geometry, and subject-specific versus average material properties altered localised AT stresses for tendinopathic tendons.

2.6. Statistical analysis

Independent sample t-tests (Assuming Unequal Variances) were used to compare outcome measures between groups. A two-tailed p-value < ($\alpha = 0.05$) indicated a significant difference between the cohorts. Linear regression analysis was performed using the LinearModel.fit algorithm in MATLAB R2013a to determine how the slopes of the regression between von Mises tendon stresses at all 4000 Gauss points were influenced by each combination of subject-specific versus average geometry and material properties.

Table 1
Experimental measures of Achilles tendon resting morphology and strain under load for healthy and tendinopathic groups (n = 8 per group). *indicates significantly different from healthy control (p = 0.03).

	Healthy	Tendinopathy
At rest		
Length [mm]	62.4 ± 12.7	68.5 ± 16.1
Volume [mm^3]	3617 ± 984	5341 ± 2239
Average cross-sectional area [mm2]	57.5 ± 10.7	75.2 ± 17.8*
Under load		
Maximum voluntary isometric ankle plantarflexor torque [Nm]	140.5 ± 37.2	102.5 ± 35.1
Longitudinal strain [%]	5.9 ± 1.3	7.1 ± 2.9

3. Results

There were no significant group differences in the free AT length (Healthy AT: 62.4 ± 12.7 mm, Tendinopathic AT: 68.5 ± 16.1, t = 0.84, p = 0.42) or volume (Healthy AT: 3617 ± 984 mm^3, Tendinopathic AT: 5341 ± 2239 mm^3, t = 1.99, p = 0.07). However the average resting CSA was significantly higher for the tendinopathic compared to healthy ATs (Healthy AT: 57.5 ± 10.7 mm^2, Tendinopathic AT: 75.2 ± 17.8 mm^2, t = 2.41, p = 0.03).

The maximum voluntary isometric ankle plantarflexion torque was significantly higher for the healthy compared to tendinopathic tendons (Healthy AT: 141 ± 37 Nm, Tendinopathic AT: 103 ± 35 Nm, t = 0.84, p = 0.049). The free AT strain measured using freehand three-dimensional ultrasound was 5.9 ± 1.3% at 70%MVIC for the healthy tendons, and 7.1 ± 2.9% at 50%MVIC for the tendinopathic tendons.

The subject-specific boundary loads applied in the optimisation to determine the free AT material properties were 2288 ± 605 N for the healthy tendons (70%MVIC) and 1197 ± 406 N for the tendinopathic tendons (50%MVIC). The average subject-specific material parameter values were significantly higher for the healthy tendons compared to the tendinopathic tendons for c1 (Healthy AT: 36 ± 10, Tendinopathic AT: 11 ± 7, t = 5.80, p < 0.01) and c4 (Healthy AT: 17 ± 11, Tendinopathic AT: 4 ± 2, t = 3.19, p = 0.02). The Young's modulus (c_5) was significantly lower for the tendinopathic tendon (555 ± 176 MPa) compared to the healthy tendon (1184 ± 342 MPa) (t = −1.02, p < 0.01).

The stress distributions for the tendinopathic tendons under load (Fig. 2) showed a high degree of variability in peak stress magnitude and stress location between tendons. The peak stress magnitude was significantly lower for the tendinopathic tendons (28.9 ± 12.3 MPa) compared to the healthy tendons (70.2 ± 13.2 MPa) (t = 6.50, p < 0.01). No differences in peak stress location were detected between groups (Tendinopathy: 56 ± 16% length from calcaneus to soleus muscle-tendon junction (MTJ); Healthy: 67 ± 22% length from calcaneus to soleus MTJ) (t = 1.13, p = 0.28).

The change in local stress caused by the introduction of pathological properties to the healthy Achilles tendon is displayed in Fig. 3. Replacing the healthy material properties with tendinopathic material properties resulted in increased overall tendon stress as indicated by the slope of the regression line which was greater than 1 (Fig. 3A). In contrast, replacing the average healthy geometry with the average tendinopathic geometry resulted in an overall decrease in tendon stress as indicated by the regression slope which was below 1 (Fig. 3B). When the average geometry and material properties for the healthy tendon were replaced by average values for tendinopathic tendon, the slope of the regression line remained below 1, indicating that tendinopathic geometry has a greater influence on tendon stress than the tendinopathic material properties.

For the tendinopathic tendons, tendon stress was found to be more sensitive to variations in geometry assessed at each individuals subject-specific material properties (Fig. 4A) than variations in material properties when assessed at each individuals subject-specific tendon geometry (Fig. 4B).

4. Discussion

Previous studies reported that mid portion Achilles tendinopathy is characterised by tendon thickening (Arya and Kulig, 2010;

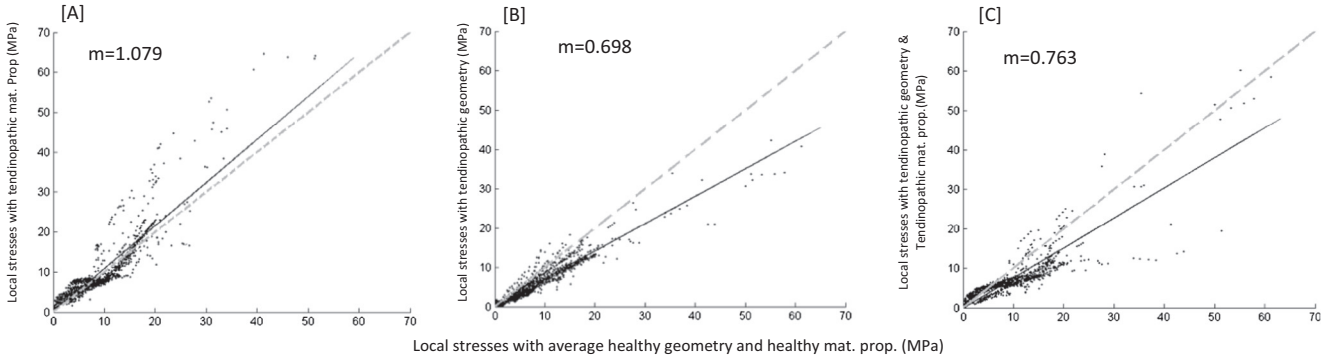

Fig. 3. Scatterplots and linear regression lines of local stresses (MPa) in the healthy tendon with healthy material properties compared to (A) with tendinopathic material properties, (B) with tendinopathic geometry and (C) with tendinopathic geometry and tendinopathic material properties. The regression line and its slope (m) are also displayed in each panel. The grey identity line represents perfect agreement.

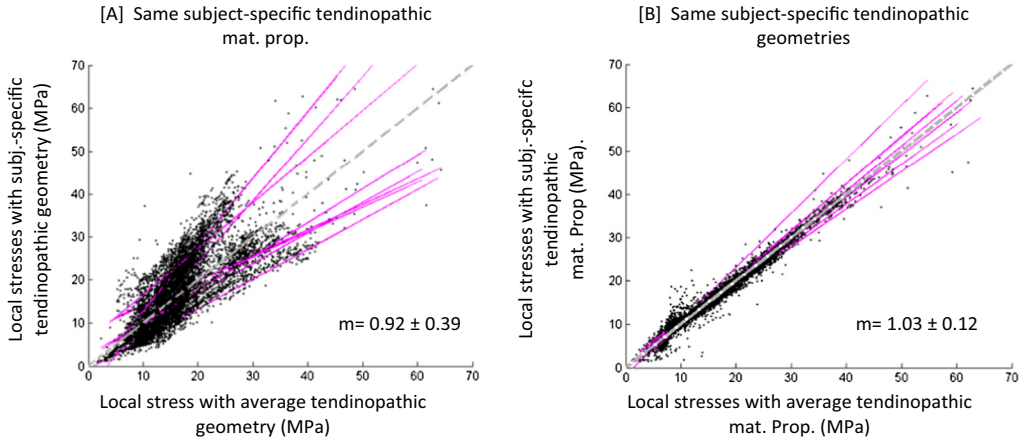

Fig. 4. Scatterplots and linear regression lines of local stresses (MPa) for combinations of subject-specific versus average geometry and material properties for tendinopathic tendons. Comparisons are for (A) tendinopathic tendon with subject-specific versus average geometry at the same subject-specific material properties, and (B) for subject specific tendinopathic tendons with subject-specific versus average material properties.

Nuri et al., 2017b, 2018) and altered material properties (Arya and Kulig, 2010). This study quantified the relative contributions of tendon thickening and decreased material properties on tissue stress under load in tendinopathic compared to healthy Achilles tendons. Subject-specific FE analyses revealed that tendinopathic Achilles tendons experienced less stress at submaximal loading compared to healthy tendons. Linear regression analysis showed that tendinopathic alterations in tendon CSA had a greater influence on local tendon stress than changes in Young's modulus. These findings suggest that the greater tendon CSA observed in tendinopathy compensates for the substantially lower Young's modulus, and thereby protects pathological tendon against excessive stress.

The resting free tendon's CSA in the present study was on average 31% greater for the tendinopathic compared to the healthy tendons, which is within the 20–66% range reported in other studies (Arya and Kulig, 2010; Nuri et al., 2017b, 2018). The mean free Achilles tendon volume was similarly greater in the tendinopathy group in the present study, although this volume difference relative to the healthy tendons only approached statistical significance ($p = 0.07$). We also found, via numerical optimisation, that the mean Young's modulus for pathological tendons was 53% lower than the corresponding value for healthy tendon. Arya and Kulig (2010) similarly reported a Young's modulus in Achilles tendinopathy that was approximately half that for healthy tendons. It was also notable from our study that there was a substantial degree of inter-subject variability in free Achilles tendon geometry and material properties within the tendinopathy group, which has been shown to be a critical determinant of tendon stress in healthy Achilles tendons (Hansen et al., 2017).

Our FE analysis based on subject-specific estimates of free AT morphology and material properties revealed that tendon stress computed at over 4000 Gauss points across the tendon was on average 24% lower in the tendinopathic compared to the healthy tendons. The lower tendon stress in tendinopathy was due to a greater influence of altered tendon CSA, which reduced tendon stress by 30%, compared to material parameters, which increased tendon stress by 8%. These findings indicate that tendon thickening in tendinopathy is a favourable biological adaptation that compensates for reduced tendon mechanical and material properties and thereby protects the tendon from excessive localised stress (Docking and Cook, 2016).

Hansen et al. (2017) and Shim et al. (2014) previously demonstrated that stress distribution in healthy Achilles tendon is more sensitive to geometry than material properties. In the present study, subject-specific variations in tendon geometry were found to have a greater effect on localised tendon stress computed at each point across the tendon than subject-specific variation in material properties. When considered together with the findings from Hansen et al. (2017) and Shim et al. (2014), the findings of the present study suggest that the stress experienced by the free Achilles tendon is highly dependent on subject-specific tendon geometry, and therefore that personalised three-dimensional tendon geometry should be an essential feature of efforts to model Achilles tendon stress.

One important practical implication of these findings is that generic rehabilitation exercises commonly prescribed to treat tendinopathy, such as eccentric heel drops (Obst et al., 2016), are likely to result in very different Achilles tendon stresses and strains for different patients. Tendon strain is an important mechanical trigger for the biological cascade regulating tendon structural adaptation (Mehdizadeh et al., 2017). The findings of this study therefore point to the need for personalised training and rehabilitation for the Achilles tendon that takes account of the substantial variation in tendon geometry and material properties between individuals to ensure an optimal loading stimulus is provided that maximises positive tissue adaptation for healthy and tendinopathic tendons (Pizzolato et al., 2017a).

There are several limitations to our study. Firstly, we assumed that the Achilles tendon material properties were homogeneous, which does not reflect the possibility that tendon material properties could be anisotropic (Bogaerts et al., 2016) and thereby influence the local stress-strains, particularly in the region of the lesion (Chatzistergos et al., 2016). However as the spatial variations of Achilles tendon material properties are as yet unknown, and may even be homogenous in tendinopathy (Choi et al., 2016), this assumption seemed justified in the first instance. Secondly, although we were able to match global strains from our model to experimental data, validation of local strain estimates remains challenging (Maganaris et al., 2017). We also assumed that the boundary force applied to our finite element model could be represented by the measured ankle joint plantarflexion moment divided by the Achilles tendon moment arm, which neglects the effects of antagonistic co-contraction and assumes the calculated force is fully transmitted to the Achilles tendon. Future studies may need to include subject-specific estimates of Achilles tendon moment arm which may also be assessed using freehand three-dimensional ultrasound (Obst et al., 2017) and include more detailed muscle force representations via musculoskeletal modelling approaches (Pizzolato et al., 2015; Pizzolato et al., 2017b). The effect of more detailed representation of tendon microstructure including tendon tissue architecture and tendon twist (Pekala et al., 2017; Shim et al., 2018), as well as the effect of calcaneal rotation (Lersch et al., 2012), may also need to be included in future models. It is also conceivable that such models could operate in near real-time and help guide tendon training programs that seek to use targeted mechanical loading as a way of optimising training adaptation (Pizzolato et al., 2017a; Pizzolato et al., 2017c).

In conclusion, this study demonstrated that tendon thickening can be viewed as a positive biological adaptation in tendinopathy that compensates for diminished tendon material properties and helps protect the tendon against excessive stress. Our overall findings also confirm the strong influence of tendon geometry on tendon stress distribution and reaffirm the importance of incorporating subject-specific tendon geometry in efforts to estimate Achilles tendon stress.

Conflicts of interest

The authors have no conflicts of interest related to this study.

Acknowledgement

This work was funded by the Australian Research Council Linkage Grant (LP110100581)

References

Alfredson, H., 2003. Chronic midportion Achilles tendinopathy: an update on research and treatment. Clin. Sports Med. 22, 727–741.
Arya, S., Kulig, K., 2010. Tendinopathy alters mechanical and material properties of the Achilles tendon. J. Appl. Physiol. 1985 (108), 670–675.
Astrom, M., Rausing, A., 1995. Chronic Achilles tendinopathy. A survey of surgical and histopathologic findings. Clin. Orthop. Relat. Res., 151–164
Barber, L., Barrett, R., Lichtwark, G., 2009. Validation of a freehand 3D ultrasound system for morphological measures of the medial gastrocnemius muscle. J. Biomech. 42, 1313–1319.
Bogaerts, S., Desmet, H., Slagmolen, P., Peers, K., 2016. Strain mapping in the Achilles tendon – a systematic review. J. Biomech. 49, 1411–1419.
Chatzistergos, P., Maganaris, C., Chockalingam, N., 2016. Sensitivity of a numerical model to detect regional differences in mechanical properties of tendons. J. Foot Ankle Surg. 22, 15.
Choi, R.K., Smith, M.M., Martin, J.H., Clarke, J.L., Dart, A.J., Little, C.B., Clarke, E.C., 2016. Chondroitin sulphate glycosaminoglycans contribute to widespread inferior biomechanics in tendon after focal injury. J. Biomech. 49, 2694–2701.
Docking, S.I., Cook, J., 2016. Pathological tendons maintain sufficient aligned fibrillar structure on ultrasound tissue characterization (UTC). Scand. J. Med. Sci. Sports 26, 675–683.
Hansen, W., Shim, V.B., Obst, S., Lloyd, D.G., Newsham-West, R., Barrett, R.S., 2017. Achilles tendon stress is more sensitive to subject-specific geometry than subject-specific material properties: a finite element analysis. J. Biomech. 56, 26–31.
Helland, C., Bojsen-Moller, J., Raastad, T., Seynnes, O.R., Moltubakk, M.M., Jakobsen, V., Visnes, H., Bahr, R., 2013. Mechanical properties of the patellar tendon in elite volleyball players with and without patellar tendinopathy. Br. J. Sports Med. 47, 862–868.
Horgan, C.O., Knowles, J.K., 1983. Recent developments concerning Saint-Venant's Principle. In: Hutchinson, J.W., Wu, T.Y. (Eds.), Advances in Applied Mechanics. Elsevier, pp. 179–269.
Hsu, P.W., Prager, R.W., Gee, A.H., Treece, G.M., 2006. Rapid, easy and reliable calibration for freehand 3D ultrasound. Ultrasound. Med. Biol. 32, 823–835.
Khan, K.M., Cook, J.L., Bonar, F., Harcourt, P., Astrom, M., 1999. Histopathology of common tendinopathies. Update and implications for clinical management. Sports Med. 27, 393–408.
Kongsgaard, M., Aagaard, P., Kjaer, M., Magnusson, S.P., 2005. Structural Achilles tendon properties in athletes subjected to different exercise modes and in Achilles tendon rupture patients. J. Appl. Physiol. 1985 (99), 1965–1971.
Kongsgaard, M., Nielsen, C.H., Hegnsvad, S., Aagaard, P., Magnusson, S.P., 2011. Mechanical properties of the human Achilles tendon, in vivo. Clin. Biomech. (Bristol, Avon) 26, 772–777.
Lersch, C., Grotsch, A., Segesser, B., Koebke, J., Bruggemann, G.P., Potthast, W., 2012. Influence of calcaneus angle and muscle forces on strain distribution in the human Achilles tendon. Clin. Biomech. (Bristol, Avon) 27, 955–961.
Leung, J.L., Griffith, J.F., 2008. Sonography of chronic Achilles tendinopathy: a case-control study. J. Clin. Ultrasound. 36, 27–32.
Maffulli, N., Sharma, P., Luscombe, K.L., 2004. Achilles tendinopathy: aetiology and management. J. R. Soc. Med. 97, 472–476.
Maganaris, C.N., Chatzistergos, P., Reeves, N.D., Narici, M.V., 2017. Quantification of internal stress-strain fields in human tendon: unraveling the mechanisms that underlie regional tendon adaptations and mal-adaptations to mechanical loading and the effectiveness of therapeutic eccentric exercise. Front. Physiol. 8, 91.
Mehdizadeh, A., Gardiner, B.S., Lavagnino, M., Smith, D.W., 2017. Predicting tenocyte expression profiles and average molecular concentrations in Achilles tendon ECM from tissue strain and fiber damage. Biomech. Model. Mechanobiol. 16, 1329–1348.
Nuri, L., Obst, S.J., Newsham-West, R., Barrett, R.S., 2017a. Regional three-dimensional deformation of human Achilles tendon during conditioning. Scand. J. Med. Sci. Sports 27, 1263–1272.
Nuri, L., Obst, S.J., Newsham-West, R., Barrett, R.S., 2017b. The tendinopathic Achilles tendon does not remain iso-volumetric upon repeated loading: insights from 3D ultrasound. J. Exp. Biol. 220, 3053–3061.
Nuri, L., Obst, S.J., Newsham-West, R., Barrett, R.S., 2018. Three-dimensional morphology and volume of the free Achilles tendon at rest and under load in people with unilateral mid-portion Achilles tendinopathy. Exp. Physiol. 103, 358–369.
Obst, S.J., Barber, L., Miller, A., Barrett, R.S., 2017. Reliability of achilles tendon moment arm measured in vivo using freehand three-dimensional ultrasound. J. Appl. Biomech. 33, 300–304.
Obst, S.J., Heales, L.J., Schrader, B.L., Davis, S.A., Dodd, K.A., Holzberger, C.J., Beavis, L. B., Barrett, R.S., 2018. Are the mechanical or material properties of the achilles and patellar tendons altered in tendinopathy? A systematic review with meta-ANALYSIS. Sports Med. 48, 2179–2198.
Obst, S.J., Newsham-West, R., Barrett, R.S., 2014a. In vivo measurement of human achilles tendon morphology using freehand 3-D ultrasound. Ultrasound. Med. Biol. 40, 62–70.
Obst, S.J., Newsham-West, R., Barrett, R.S., 2016. Changes in Achilles tendon mechanical properties following eccentric heel drop exercise are specific to the free tendon. Scand. J. Med. Sci. Sports 26, 421–431.
Obst, S.J., Renault, J.B., Newsham-West, R., Barrett, R.S., 2014b. Three-dimensional deformation and transverse rotation of the human free Achilles tendon in vivo during isometric plantarflexion contraction. J. Appl. Physiol. 1985 (116), 376–384.
Pekala, P.A., Henry, B.M., Ochala, A., Kopacz, P., Taton, G., Mlyniec, A., Walocha, J.A., Tomaszewski, K.A., 2017. The twisted structure of the Achilles tendon unraveled: a detailed quantitative and qualitative anatomical investigation. Scand. J. Med. Sci. Sports 27, 1705–1715.

Pizzolato, C., Lloyd, D.G., Barrett, R.S., Cook, J.L., Zheng, M.H., Besier, T.F., Saxby, D.J., 2017a. Bioinspired technologies to connect Musculoskeletal Mechanobiology to the person for training and rehabilitation. Front. Comput. Neurosci. 11, 96.

Pizzolato, C., Lloyd, D.G., Sartori, M., Ceseracciu, E., Besier, T.F., Fregly, B.J., Reggiani, M., 2015. CEINMS: a toolbox to investigate the influence of different neural control solutions on the prediction of muscle excitation and joint moments during dynamic motor tasks. J. Biomech. 48, 3929–3936.

Pizzolato, C., Reggiani, M., Modenese, L., Lloyd, D.G., 2017b. Real-time inverse kinematics and inverse dynamics for lower limb applications using OpenSim. Comput. Methods Biomech. Biomed. Eng. 20, 436–445.

Pizzolato, C., Reggiani, M., Saxby, D.J., Ceseracciu, E., Modenese, L., Lloyd, D.G., 2017c. Biofeedback for gait retraining based on real-time estimation of tibiofemoral joint contact forces. IEEE Trans. Neural. Syst. Rehabil. Eng. 25, 1612–1621.

Robinson, J.M., Cook, J.L., Purdam, C., Visentini, P.J., Ross, J., Maffulli, N., Taunton, J.E., Khan, K.M., Victorian Institute Of Sport Tendon Study, G., 2001. The VISA-A questionnaire: a valid and reliable index of the clinical severity of Achilles tendinopathy. Br. J. Sports Med. 35, 335–341.

Rolf, C., Movin, T., 1997. Etiology, histopathology, and outcome of surgery in achillodynia. Foot Ankle Int. 18, 565–569.

Shim, V.B., Fernandez, J.W., Gamage, P.B., Regnery, C., Smith, D.W., Gardiner, B.S., Lloyd, D.G., Besier, T.F., 2014. Subject-specific finite element analysis to characterize the influence of geometry and material properties in Achilles tendon rupture. J. Biomech. 47, 3598–3604.

Shim, V.B., Besier, T.F., Lloyd, D.G., Mithraratne, K., Fernandez, J.F., 2016. The influence and biomechanical role of cartilage split line pattern on tibiofemoral cartilage stress distribution during the stance phase of gait. Biomech. Model. Mechanobiol. 15, 195–204.

Shim, V.B., Handsfield, G.G., Fernandez, J.W., Lloyd, D.G., Besier, T.F., 2018. Combining in silico and in vitro experiments to characterize the role of fascicle twist in the Achilles tendon. Sci. Rep. 8, 13856.

Treece, G.M., Gee, A.H., Prager, R.W., Cash, C.J., Berman, L.H., 2003. High-definition freehand 3-D ultrasound. Ultrasound. Med. Biol. 29, 529–546.

Treece, G.M., Prager, R.W., Gee, A.H., Berman, L., 1999. Fast surface and volume estimation from non-parallel cross-sections, for freehand three-dimensional ultrasound. Med. Image Anal. 3, 141–173.

Weiss, J.A., Maker, B.N., Govindjee, S., 1996. Finite element implementation of incompressible, transversely isotropic hyperelasticity. Comput. Methods Appl. Mech. Eng. 135, 107–128.